Structures 40 (2022) 64–73

Contents lists available at ScienceDirect

Structures

journal homepage: www.elsevier.com/locate/structures

Topology optimization of truss structure considering nodal stability and local buckling stability

Qi Cai, Ruoqiang Feng *, Zhijie Zhang

Key Laboratory of Concrete and Prestressed Concrete Structures of Ministry of Education, Southeast University, Nanjing, Jiangsu Province 211189, China

ARTICLE INFO

Keywords:
Structural optimization
Truss
Local buckling
Nodal stability
Linear programming

ABSTRACT

In order to obtain stable and realistic truss structures in practical applications, it is essential to include nodal and local buckling stability in truss topology optimization. There have been several approaches to address the challenges including nodal stability or local buckling stability. However, these approaches often lead to ill-conditioned optimization problems, such as convergence problems due to the concavity of the problem or high computational costs. In this study, two novel but conceptually simple methodologies, the nominal perturbing force (NPF) approach, and the allowable stress iteration (ASI) approach, are proposed to address nodal instability and local buckling instability problems in truss topology optimization, respectively. Initially, in the NPF approach, an infinite number of disturbing forces that a node may suffer are incorporated into the truss topology optimization problem in the form of nominal perturbing force conditions, whose magnitude and direction are discussed to capture the worst case. In the ASI approach, the allowable stress for each compressive bar is redefined in each iteration to ensure that the Euler critical buckling constraint is active. In this way, the concave local buckling instability problem is linearized in each iteration and can be solved efficiently by a linear programming solver. Finally, based on the finite element limit analysis (FELA) method, a truss topology optimization formulation incorporating the NPF and ASI approaches is proposed to solve the nodal stability and local buckling stability problems simultaneously. The proposed formulation is demonstrated through several numerical examples showing significant effects of including nodal stability and local buckling stability in the optimized designs, while at the same time demonstrating the validity and potential of the proposed approaches.

1. Introduction

The pin-jointed truss topology (or "layout") optimization problem is concerned with finding an optimal arrangement of structural bars subject to prescribed constraints. A typical truss topology optimization problem might comprise a design domain containing an array of fixed nodal points connected by potential members, called the ground structure [4,11,33,37,42]. The optimization objective might typically then be to minimize the total volume, mass [21,37], or compliance[28] of structure, with constraints ensuring that each node is in static equilibrium and that bar stresses are within predefined limits [22,47,48]. The optimal cross-sectional areas for all the bars in the ground structure are then determined as part of the optimization process; typically, many of these will be zero, leaving the optimal topology comprising only of bars with non-zero cross-sectional areas[20].

Mathematically, the ground structure provides a feasible domain for the truss structure optimization problem. Typically, the truss topology optimization based on the ground structure method is mainly divided into four steps [19]. Firstly, as shown in Fig. 1a, the design domain with appropriate supports and loads is determined. Secondly, as shown in Fig. 1b, the nodes are arranged, usually evenly, to discrete the design domain. Thirdly, as shown in Fig. 1c, these nodes are connected with potential bars to generate the ground structure. Finally, as shown in Fig. 1d, some optimization algorithms are used to remove the redundant bars to generate the optimal structure.

However, the optimized structure obtained by using the ground structure method always contains unstable nodes [12,49] within successive parallel compression bars, such as node N_5 in Fig. 1d. When the unstable nodes are disturbed by external forces, it may lead to structural instability, which is not allowed in the structural design.

In previous studies, lots of attempts had been made to solve the nodal instability problem. As shown in Fig. 2, an intuitive approach is to eliminate unstable nodes directly and then merge these consecutive bars into a single long bar whose length is equal to the sum of the lengths of the merged bars [1].

* Corresponding author.
E-mail address: hitfeng@163.com (R. Feng).

https://doi.org/10.1016/j.istruc.2022.04.008
Received 24 February 2022; Received in revised form 1 April 2022; Accepted 2 April 2022
Available online 9 April 2022

Nomenclature

N_n	Number of nodes
d	Dimension of Euclidean space
N_s	Number of supports
N_{dof}	Number of degrees of freedom of the nodes
N_b	Number of bars
$\mathbf{a}$	Vector of cross-sectional areas
$\mathbf{l}$	Vector of bar lengths
$\mathbf{B}$	Equilibrium matrix
$\mathbf{q}^t$	Matrix of axial force
$\mathbf{f}^t$	Matrix of external loads
$\mathbf{f}^x$	Vector of nominal perturbing force along x-axis
$\mathbf{f}^y$	Vector of nominal perturbing force along y-axis
d^x	Vector of bar cosines perpendicular to the x-axis
d^y	Vector of bar cosines perpendicular to the y-axis
f_j^x	Vector of nominal perturbing force along x-axis at node j
f_j^y	Vector of nominal perturbing force along y-axis at node j
V	Volume of structure
σ^+	Limiting tensile yield stresses
σ^-	Limiting compressive yield stresses
r	Nominal perturbing force coefficient
P_i^{cr}	Critical buckling load of the bar i
I	Second moment of inertia of cross sections
E	Young's modulus of material
σ_i^k	Stress in the bar i at iteration k
a_i^{cr}	Critical buckling area of the bar i
i	truss bar
t	External load cases
V^k	Volume of structure at iteration k
ε	Volume convergence value
f^x	Nominal perturbing force along x-axis
f^y	Nominal perturbing force along y-axis
M	Number of external load cases

However, as Rozvany [38] observed, the inclusion of local buckling in an optimization formulation means that any method which involves this approach is highly unlikely to obtain an optimal design. This is because the critical buckling strength of the longer merged bar will typically be significantly lower than those of any original parallel consecutive compression bars due to the longer length of the bars. As a result, the required cross-sectional area of the new generated long bar will need to be larger than any of the original bars, as shown in Fig. 2c. To avoid bar local buckling, it is usually necessary to increase the cross-section of the newly generated long bar, which may result in a less-optimized structure. In a similar vein, Smoekh and Kirsch [40] proposed an interactive iterative approach, whereby the analysis would identify mechanisms and insert additional members to stabilize unstable nodes.

Another approach is to add constraints on the minimum number of active bars (two for planar trusses and three for spatial trusses) connected to the active nodes in the truss topology optimization problem [6,34]. The original intention of this approach is to add enough bracings to the unstable nodes to limit the node motion. However, in this approach, it may be neither guaranteed that all directions of freedom of the nodes are constrained nor that the bracings can provide sufficient support forces.

The inclusion of a global elastic stability criterion [13,24,27] in the optimization algorithm can also, to some extent, solve the nodal stability problem in truss topology optimization, since the global stability of the structure requires nodal stability by default. However, due to the low computational efficiency of solving the semidefinite programming, only ground structures containing a relatively small number of bars can be solved in this way.

Another approach is to include imperfections in the ground structure, such as nodal displacements or forces generated in the optimization. The robust optimization method [2,32] is first be proposed to solve a problem in which all possible perturbing forces with a small given magnitude are applied to any or all nodes in the ground structure. The

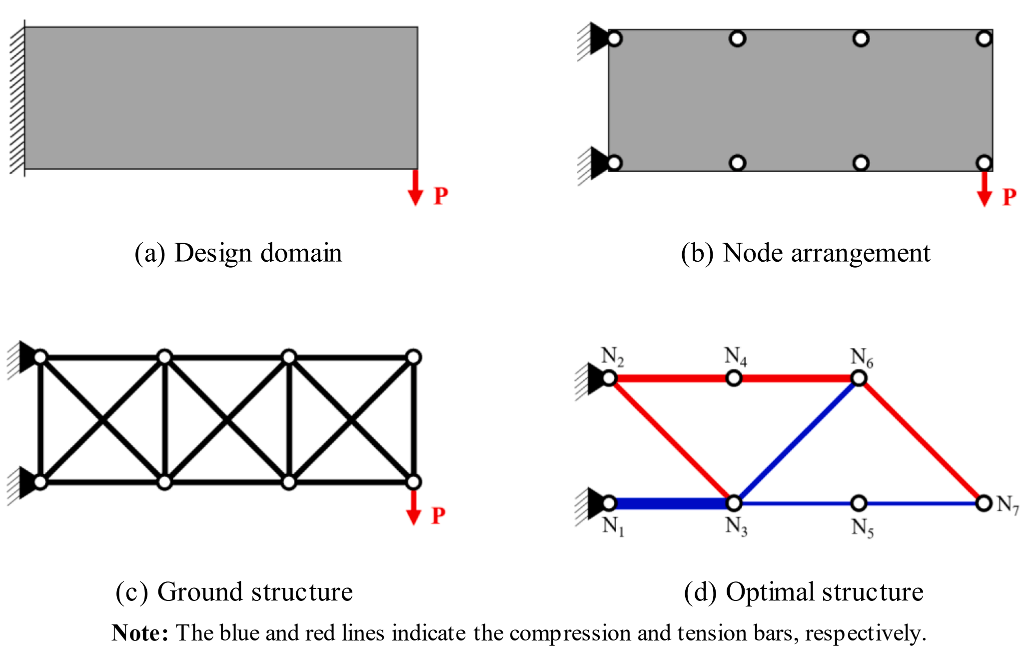

Fig. 1. Optimization of truss structure based on ground structure method. **Note:** The blue and red lines indicate the compression and tension bars, respectively. (For interpretation of the references to colour in this figure legend, the reader is referred to the web version of this article.)

disadvantage of this approach is that any node to which a perturbing force is applied must become part of the final optimized structure since the perturbing force must be constrained by bars or supports. However, usually, most nodes in the original ground structure will not be included in the final optimized structure. Consequently, Ben-Tal and Nemirovski [3] have proposed a two-stage approach, finding an optimized but unstable structure firstly, then applying the perturbation forces to only those nodes which are active in this structure. However, whilst the method will obtain a properly stabilized solution, by only including the nodes identified in the first step, many considerably optimal solutions will be missed [41].

Another widely used method is the nominal lateral force (NLF) method [10,31,41], which is similar to the robust design optimization method, except that deterministic loadings are considered instead: the method adds to the primary loading cases some small occasional perturbation loadings called nominal force cases. The magnitude of these perturbation loadings is scaled by the braced compression forces in the consecutive compression bars, whose principle can be found in most practical design codes [7,18,17]. The NPF approach is first proposed in Winter's method [43] for the design of steel columns and beams. Tyas and Gilbert [41] first introduced this method to the field of truss topology optimization and presented an optimization model for truss structures with constraints on stress and local buckling. To consider node displacements, Descamps and Coelho [10] introduced the nominal force method to simultaneous geometry and topology optimization and proposed an optimization model using mixed-integer programming. However, in order to apply nominal forces only at the unstable nodes within the compression bars, two variables are required to represent the axial force of any bar, which significantly increases the computational cost. Therefore, in order to improve the computational efficiency, the nominal perturbing force (NPF) method is proposed in this paper.

The remainder of the paper is ordered as follows. Section 2 begins with the basic problem statement by using finite element limit analysis (FELA) formulation for truss topology optimization [23]. The NPF approach and the ASI method are then derived and adapted for nodal stability constraints and local buckling stability constraints, respectively, leading to the main contribution of this work: a novel FELA formulation for truss topology optimization incorporating stability considerations. In section 3, three numerical examples are presented to illustrate the applicability of the method. Finally, concluding remarks are given in Section 4 along with further prospects to improve the method.

2. Truss topology optimization

For convenience, the structures studied in this section are plane trusses defined by N_n nodal points and N_b bars. For spatial trusses, there is a similar derivation. The number of supports is denoted N_s and the number of degrees of freedom of the nodes is $N_{dof} = d \times N_n - N_s$, where $d = 2$ for plane truss and $d = 3$ for special truss. The sectional area of the bar i is given as a_i collected in $\mathrm{a} \in \mathrm{R}^{N_b \times 1}$. Similarly, the lengths of bars are collected in $\mathrm{l} \in \mathrm{R}^{N_b \times 1}$. Therefore, the volume of total truss is thus given by.

$$V = \sum_{i=1}^{N_b} a_i l_i = \mathrm{a}^T l$$

where V is the total volume of the structure, l_i is the length of the bar i.

2.1. Finite element limit analysis

The Finite element limit analysis (FELA) method [9,26,35] is based on the finite element method (FEA), as all variables, equations and inequalities are either node or bar based. The material models in the FEA are simplified assuming a rigid behavior prior to plasticity, i.e., a perfect plastic material. However, the load-defection path is not determined, as no deformations occur before yielding. Moreover, unlimited deformation capacity is assumed, only the collapse model is found, and small displacements are assumed. For more introduction to FELA, readers can refer to [9,25,35,36].

Therefore, based on the FELA method, the plastic formulation [14,15,46,45] for the minimized truss volume with nodal equilibrium and bar stress constraints subjected to M external load conditions can be formulated as.

$$\begin{aligned} &\min_{\mathrm{a},q} V = \mathrm{a}^T \mathrm{l} \\ &\text{s.t. } \mathrm{Bq}^t = \mathrm{f}^t \qquad t = 1, 2, \ldots, M, \ i = 1, 2, \ldots, N_b \\ &-\sigma^- a_i \leqslant q_i^t \leqslant \sigma^+ a_i \ a_i \geqslant 0 \end{aligned} \tag{1}$$

where $\mathrm{B} \in \mathrm{R}^{N_{dof} \times N_b}$ is the equilibrium matrix, built from the directional cosines of the bars, $\mathrm{q}^t \in \mathrm{R}^{N_b \times M}$ is a matrix containing the axial force for all bars under M external load conditions, and $\mathrm{f}^t \in \mathrm{R}^{N_{dof} \times M}$ is a matrix containing the external loads, $\sigma^+ > 0$ and $\sigma^- > 0$ are limiting tensile and compressive yield stresses respectively, q_i^t is the axial force of the bar i under loading case f^t.

The optimization variables are the cross-sectional areas in **a** and the internal force in **q**. It can be observed that the element in matrix **B** is determined by the positions and connectivity of the nodes in the ground structure. Therefore, the optimization formulation is a linear programming problem, which can be solved very efficiently by a state-of-the-art solver.

2.2. Nominal perturbing force approach

In order to address the nodal instability problem in the optimized structure, the novel NPF approach is proposed in this study. In the NPF approach, an infinite number of disturbing forces at nodes in the ground structure are incorporated into the truss topology optimization problem in the form of nominal perturbing force conditions, whose magnitude and direction will be determined in the following section.

2.2.1. Magnitude of the nominal perturbing force

A given node in a two-dimensional plane truss has a degree of freedom along each of two mutually orthogonal axes (for simplicity these will be assumed to be coincident with the usual Cartesian axes). Considering a single primary external load case, each of these axes is considered in turn with the sum of all the components of axil forces pushing onto the node normal to this axis being determined, and a nominal force taken as some specified proportion of this sum.

Using the two-bar structure shown in Fig. 3 as an example, the nominal perturbing forces can be calculated from the following equation,

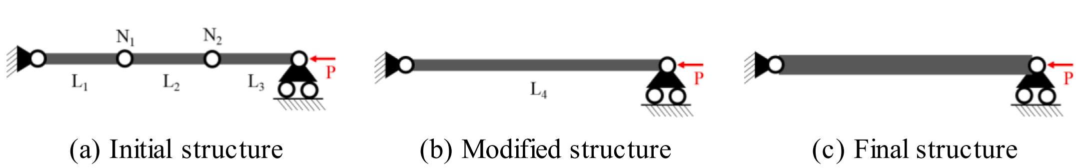

Fig. 2. Remove unstable node method.

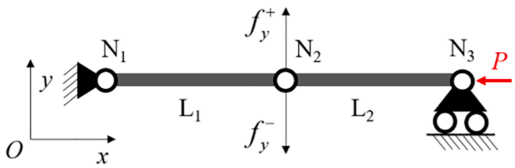

Fig. 3. Two-bar structure parallel to the coordinate axis.

$$f_y^+ = f_y^- = \frac{1}{2} r \sum_{i=1}^{m_j} q_i d_i^x \tag{2}$$

where f_y^+ and f_y^- are two nominal perturbing force conditions at node N_2 in the same and opposite directions to the y-axis, respectively, m_j is the number of bars connected to node j, d_i^x is the direction cosine of the bar i relative to the x-axis, r is the nominal perturbing force coefficient, which reflects the ratio of the magnitude of the bracing force to the axial force of the braced bars. In this paper, the nominal perturbing force calculated by using formula (2) is called calculated nominal force.

The magnitude of the perturbing force required to stabilize the internal nodes within compressive bars has been studied for half a century. In the 1960 s, Winter [43] first determined the influence of the stiffness of the bracing on the determination of the bracing forces. However, as Yura [44] pointed out, the magnitude of the bracing force in the bracing is dominated by the magnitude of the compression force and the degree of geometric imperfections of braced bars rather than the stiffness of the bracings. This is mainly reflected in the requirements of the practical design code that stipulates the strength standards of bracings. For example, GB 50017-2017 [7] requires that when the bracing is located in the middle of the braced bar, the bracing force should be no less than 1/60 of the compressive force being resisted. In addition, both BS5950 [18] and EC3 code [17] require that, in general, the bracing force should be not less than 1% of the compression force that is being resisted. It is clear that the bracing force should be not less than a small percentage of the compression force of the braced bar. Therefore, in this study, the magnitude of the nominal perturbing force perpendicular to the braced bars is taken as 1% of the magnitude of the compression force of the braced bars.

2.2.2. Direction of the nominal perturbing force

In practical engineering, the nodes of the trusses may be subjected to disturbing forces in any direction. However, it is impossible to set the perturbing forces in arbitrary directions in the optimization of truss structures. Therefore, to simplify the calculations, the directions of the nominal perturbing force conditions are set to coincide with each of the Cartesian axis directions separately, as proposed by Tyas et al. [41] in the NPF approach.

However, when the orientation of the bars does not necessarily coincide with the Cartesian axis, one of the main concerns is how to evaluate the direction and magnitude of the nominal perturbing forces. In the following, we discuss this issue using the two-bar structure shown in Fig. 4. Four perturbing force conditions are applied to node N_2, which are load conditions f^x and $-f^x$ along with the positive and negative directions of the x-axis, and f^y and $-f^y$ along with the positive and negative directions of the y-axis, respectively. According to formula (2), the perturbing forces can be stated as,

$$f^x = rP\sin\alpha \quad \alpha \in \left[0,\ \frac{\pi}{2}\right] \tag{3}$$

$$f^y = rP\cos\alpha \quad \alpha \in \left[0,\ \frac{\pi}{2}\right] \tag{4}$$

where P is the axial force of the compression bar, α is the angle between the bar and the x-axis. Then, the maximum component forces of the nominal perturbing force perpendicular to the bars L_1 and L_2 can be given as.

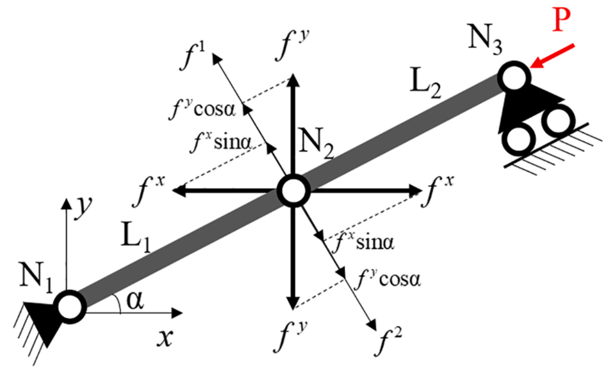

Fig. 4. Two-bar structure not parallel to the coordinate axis.

$$f^1 = f^2 = \max\{rf^x\sin\alpha, rf^y\cos\alpha\} \quad \alpha \in \left[0,\ \frac{\pi}{2}\right] \tag{5}$$

Adding Eqs. (3) and (4) to Eq. (5), the nominal perturbing force perpendicular to the braced bars can be stated as.

$$f^1 = f^2 = \max\{rP\sin^2\alpha, rP\cos^2\alpha\} \quad \alpha \in \left[0,\ \frac{\pi}{2}\right] \tag{6}$$

Therefore, as the angle between the bar and the Cartesian coordinate axis varies from 0 to $\frac{\pi}{2}$, the perturbing force perpendicular to the braced bars can be stated as.

$$\frac{1}{2} rP \leqslant f^1 = f^2 \leqslant rP \tag{7}$$

This shows that when the bar dose not coincide with any Cartesian coordinate axis, the effective component of nominal force in the direction perpendicular to the bar axis is 0.5 to 1 times the calculated nominal force. According to equation (6), when the angle α is $\frac{\pi}{4}$, the nominal force perpendicular to the direction of the bar obtains the minimum value, which is 0.5 times the calculated nominal force.

In this study, as an approximation, four nominal perturbing forces cases projected in either direction to the two Cartesian axes in plane truss are adopted. To ensure the axial force that can be provided by the bracing is at least 0.01 times the axial force of the braced bar, the nominal perturbing force coefficient r is taken as 0.02.

2.3. Local buckling constraint

In the design of structures, the local buckling stability is a critical issue. Therefore, it is very necessary for this issue to be considered in truss topology optimization. By introducing the critical Euler buckling load for a simply supported bar, the local buckling constraint for the bar i can be given as.

$$-q_i \leqslant P_i^{cr} = \frac{\pi^2 E I_i}{l_i^2} \tag{8}$$

where P_i^{cr} and I_i are the critical buckling load and the second moment of the sectional area of the bar i, respectively, E is Young's modulus. For the tension bar, formulation (8) is automatically satisfied since the axial force $q_i \geqslant 0$. Therefore, inequality (8) is only active for the compression bars. For a bar with a solid circular section, the second moment of sectional area can be expressed as,

$$I_i = \frac{a_i^2}{4\pi} \tag{9}$$

Adding the second moment of sectional area (9) into the local buckling constraint, the critical buckling area can be expressed as,

$$a_i^{cr} = \sqrt{\frac{4P_i^{cr} l_i^2}{\pi E}} \tag{10}$$

Obviously, the critical buckling load is a concave function on the cross-sectional area, which is difficult to obtain the optimal solution by using traditional Linear Programming optimization solver, directly. Therefore, in this study, a novel iteration approach is used to make the local buckling problem into a linear expression on the cross-sectional area, as shown in Fig. 5.

where $|\Delta V|$ is the change in structural volume between four consecutive iteration steps, which can be expressed as.

$$|\Delta V| = \left|\left(V^k + V^{k-1}\right) - \left(V^{k-2} + V^{k-3}\right)\right| \tag{11}$$

where V^k, V^{k-1}, V^{k-2}, V^{k-3} ($k \geqslant 4$) are the volume of structure at iteration k, k-1, k-2 and k-3, respectively. Compared with the convergence approach that only considers the change of structural volume between two consecutive iterations, this method takes into account the influence of iteration history on the convergence and ensures the stability of the convergence [5,16,29,30]. In addition, ε is taken as 0.001 in this study.

If the convergence criteria are not met, for each bar that is active in the solution, the limiting compressive yield stress for the next iteration $k+1$ can be obtained by.

$$\sigma_i^{k+1} = \sigma_i^k \frac{a_i}{a_i^{cr}} \tag{12}$$

where σ_i^k is the compressive stress in the bar i at iteration k, a_i^{cr} is the critical buckling area of the bar i, which can be stated as.

$$a_i^{cr} = \sqrt{\frac{4|q_i^k| l_i^2}{\pi E}} \tag{13}$$

where q_i^k is the axial force of the bar i at iteration k, indicates the absolute value. However, direct use of σ_i^{k+1} obtained by (12) in the iterations is likely to cause cycling to occur. Therefore, a relaxation term η, the value of which is to be taken within zero to one, is introduced in the calculation, then the limiting compressive stress can be expressed as.

$$\sigma_i^{k+1} = \eta\sigma_i^k \frac{a_i}{a_i^{cr}} + (1-\eta)\sigma_i^k \tag{14}$$

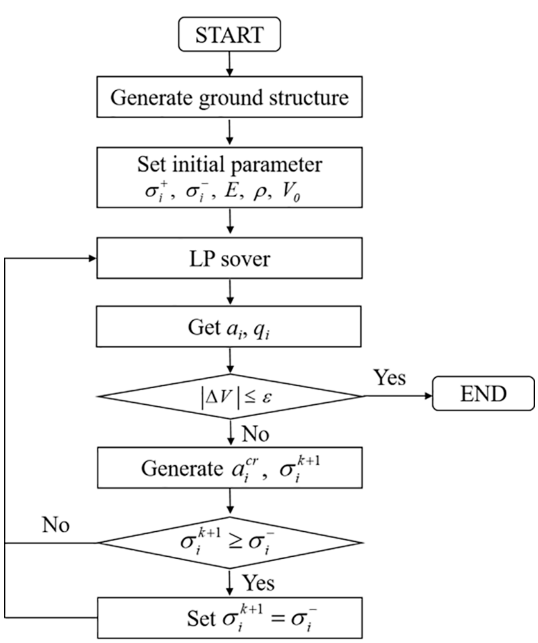

Fig. 5. Flowchart of ASI method.

For bars with other sectional areas, it is sufficient to modify the second moment formula (9).

It should be noted that the cross-sectional area of the bracing is generally small, and the minimum cross-sectional area of the bar is limited in the structure design according to some codes [8,17]. Therefore, in this study, the local buckling of the bracing bar is not considered.

2.4. Novel formulation including nodal and bar local buckling stability constraints

As discussed in the previous sections, the topology optimization problem with the constraints on local buckling stability and nodal stability can be stated as,

$$\begin{aligned}
&\min_{\mathrm{a},q} V = \mathrm{a}^T \mathrm{l} \\
&\text{s.t.} \quad \begin{array}{l}
\mathrm{B}\mathrm{q}^t = \mathrm{f}^t \\
\mathbf{B}\mathbf{q}^{M+1} = \mathbf{f}^x \\
\mathbf{B}\mathbf{q}^{M+2} = -\mathbf{f}^x \\
\mathbf{B}\mathbf{q}^{M+3} = \mathbf{f}^y \\
\mathbf{B}\mathbf{q}^{M+4} = -\mathbf{f}^y \\
\mathbf{f}^x \geqslant -\frac{1}{2} r \mathbf{q}^t \mathbf{d}^y \\
\mathbf{f}^y \geqslant -\frac{1}{2} r \mathbf{q}^t \mathbf{d}^x \\
\mathbf{f}^x \geqslant \mathbf{O} \\
\mathbf{f}^y \geqslant \mathbf{O} \\
-\sigma^- a_i \leqslant q_i^{t+4} \leqslant \sigma^+ a_i \\
a_i \geqslant 0
\end{array} \qquad t = 1, \dots, M, \quad i = 1, 2, \dots, N_b
\end{aligned} \tag{15}$$

where $\mathbf{f}^x = \left\{\mathbf{f}_1^x, \mathbf{f}_2^x, \dots, \mathbf{f}_{dof}^x\right\}^T \in \mathrm{R}^{N_{dof}\times 1}$, $\mathbf{f}^y = \left\{\mathbf{f}_1^y, \mathbf{f}_2^y, \dots, \mathbf{f}_{dof}^y\right\}^T \in \mathrm{R}^{N_{dof}\times 1}$, and for a given node j, $\mathbf{f}_j^x = \left\{f_j^x, 0\right\}^{\mathrm{T}} \in \mathrm{R}^{d\times 1}$, $\mathbf{f}_j^y = \left\{0, f_j^y\right\}^{\mathrm{T}} \in \mathrm{R}^{d\times 1}$, where f_j^x, f_j^y are the magnitudes of the nominal perturbing forces in the x- and y-directions, respectively. $\mathbf{d}^x \in \mathrm{R}^{N_b\times 1}$ and $\mathbf{d}^y \in \mathrm{R}^{N_b\times 1}$ are vectors of bar cosines required to determine the component of force at each node perpendicular to the x- and y-axis respectively. Also, $\mathrm{O} \in \mathrm{R}^{N_{dof}\times 1}$ is a vector in which all elements are all zero required to make the nodal perturbing force not less than zero in each direction at all nodes.

3. Numerical applications

The presented method for truss topology optimization, including nodal and local buckling stability, is applied to three different structures. Firstly, a simple plane truss structure is studied. The effectiveness of the method proposed in this paper in solving the nodal and local buckling stability problems is verified by analyzing the axial forces of the optimized structural bars. Secondly, a three-dimensional L-shaped structure subject to local and nodal stability constraints is investigated, and the optimization results are compared with those using the conventional NPF approach, showing the superiority of the NPF approach. Finally, in order to verify the effectiveness of the method proposed in this paper on the actual structural design, a three-dimensional crane structure subjected to four vertical loads is optimized and analyzed using the Q355 steel material, whose yield stress is 355 MPa.

If nothing else is stated, to simplify, the Young modulus E, limiting tensile and compressive yield stresses σ^+ and σ^- of material, and external load P are all taken as unity. In addition, the relaxation term is taken as 0.5. In the ground structures, all nodes are connected with straight potential bars to their nearest nodes in all directions. In the optimized solution, the blue, red, and green lines represent the compressive bar, the tension bar, and the bar subjected to force only under the action of the nominal perturbing force conditions (no force under the action of the external load condition *P*), respectively.

The code is implemented in Matlab R2016b, and the LP solver is Mosek version 9.2.47. Mainly results are computed on a desktop with AMD Ryzen 7 2700X Eight-Core Processor 3.70 GHz and 32.0 GB of RAM.

3.1. Cantilever beam

The well-known cantilever beam design domain [5,14,36,45] subject to a point force is studied. The design domain is rectangular with a side length ratio of 4:1, supported along the left edge and loaded with a concentrated load at the lower right corners. The design domain with boundary conditions and external force is seen in Fig. 6a, where L is taken as unity. In addition, the relaxation term is taken as 1. The ground structure with 20 bars and 10 nodes is shown in Fig. 6b. The optimized structure is shown in Fig. 6c-f.

The solution to the optimization problem without nodal or buckling stability considerations is shown in Fig. 6c with a volume of 23.999. The axial force, cross-sectional area, and critical load of the bar in the optimized structure are shown in Table 1. As seen in Fig. 6c, nodes N_3 and N_7 within the successive compression bars are unstable due to the lack of bracings in the *y*-axis direction. It should be noted that, although node N_6 is also not vertically supported, it is not an unstable node because it exists between two tensile bars. As can be seen from Table 1, in the compression bars, the magnitude of the axial forces of the bars L_2, L_{11} and L_{12} exceed their critical Euler buckling forces and are unstable.

When only the nodal stability is considered, the optimized structure with a volume of $V = 24.04$ is shown in Fig. 6d. The cross-sectional areas, axial forces, and critical buckling stresses of the bars are shown in Table 1. As seen in Fig. 6d, node N_3 is supported by bars L_3 and L_7, and node N_7 is supported by bars L_{13} and L_{17}, both of which are stable. From Table 2, it can be seen that the magnitude of the axial forces of both bars L_1 and L_6 is 3. The cross-sectional areas of bars L_3 and L_7 are 0.057 and 0.05, respectively. Therefore, the sum of the vertical bracing forces that L_3 and L_7 can provide for node N_3 is $F_{3y} = 0.057\times\sin\frac{\pi}{4} + 0.05\times\sin\frac{\pi}{4} = 0.076\ \mathrm{N} > 3\times 0.02 = 0.06$, which shows that node N_3 is stable. Similarly, node N_7 is also stable. However, it can be seen from Table 1 that most of the bars are local buckled.

When nodal stability and local buckling stability are considered simultaneously, the optimized structure with a volume of $V = 24.949$ is shown in Fig. 6e, and the cross-sectional areas, axial force, and critical buckling force are shown in Table 1. As can be seen in Fig. 6e, all nodes are supported in the optimized structure. Whether N_3 and N_7 below are stable is verified in the following. The magnitude of the axial force of both bars L_1 and L_6 are 3, then node N_3 requires a bracing force of 0.02 $\times$ 3 = 0.06. The cross-sectional area of L_3 is 0.085, which can provide a vertical bracing force of 0.06. Therefore, node N_3 is stable. Similarly, node N_7 is also stable. In addition, it can be seen from Table 1 that all the compressed bars of the optimized structure meet the local buckling constraint.

The optimization results of this numerical example show that the NPF approach and ASI method proposed in this paper can effectively solve the nodal stability and local buckling stability problems in truss optimization.

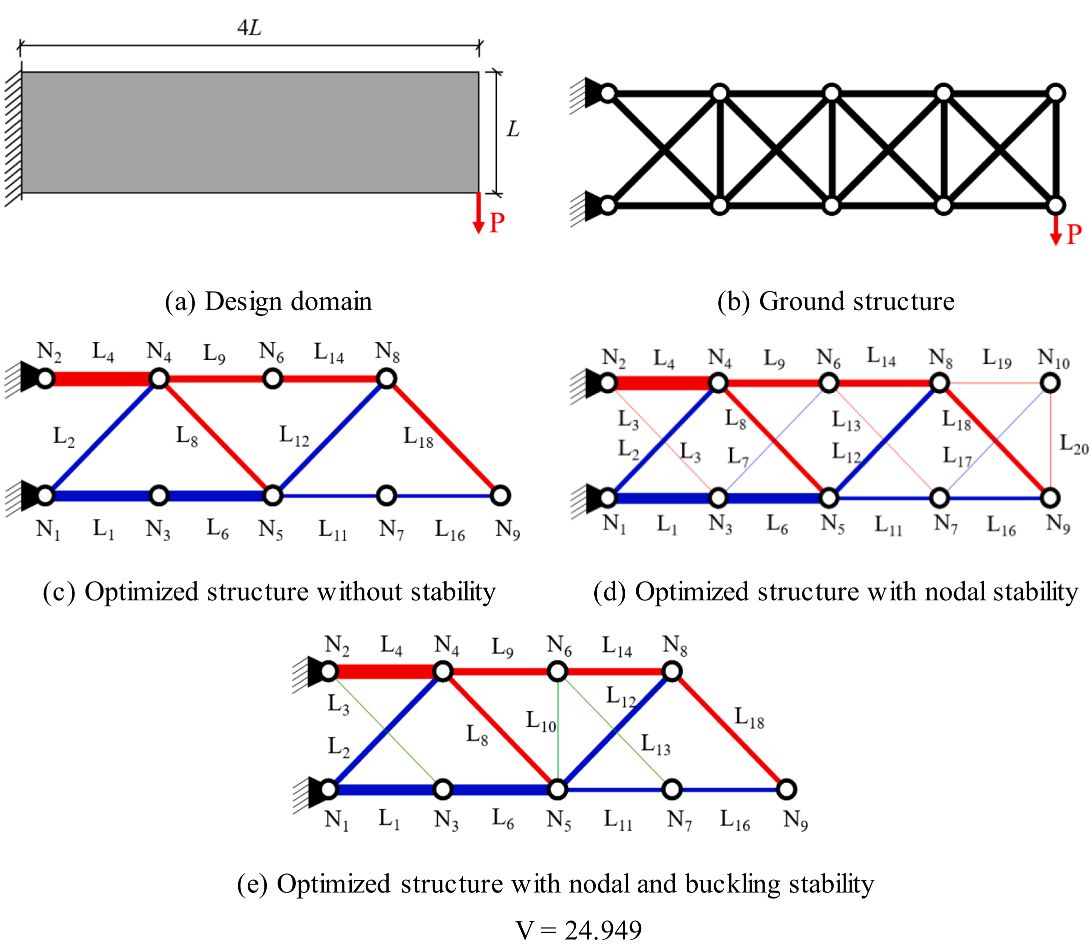

Fig. 6. Optimization of cantilever beam.

Table 1
Optimization results of cantilever beam.

		Without stability			With nodal stability			With nodal and local buckling stability		
No.	l	A	F	P_{cr}	A	F	P_{cr}	A	F	P_{cr}
L_1	1	3	−3.000	7.069	3.040	−3.040	7.069	3	−3	7.069
L_2	1.414	1.414	−1.414	1.110	1.358	−1.358	1.110	1.596	−1.414	1.415
L_3	1.414	—	—	—	0.057	0.057	—	0.085	0	—
L_4	1	4	4.000	—	3.960	3.960	—	4	4	—
L_5	1	—	—	—	—	—	—	—	—	—
L_6	1	3	−3.000	7.069	2.965	−2.965	7.069	3	−3	7.069
L_7	1.414	—	—	—	0.050	−0.050	0.001	—	—	—
L_8	1.414	1.414	1.414	—	1.364	1.364	—	1.414	1.414	—
L_9	1	2	2.000	—	2.035	2.035	—	2	2	—
L_{10}	1	—	—	—	—	—	—	0.020	0	0
L_{11}	1	1	−1.000	0.785	1.030	−1.030	0.785	1.128	−1	0.999
L_{12}	1.414	1.414	−1.414	1.110	1.372	−1.372	1.110	1.596	−1.414	1.415
L_{13}	1.414	—	—	—	0.042	0.042	—	0.028	0	0
L_{14}	1	—	—	—	1.970	1.970	—	2	2	—
L_{15}	1	—	—	—	—	—	—	—	—	—
L_{16}	1	—	—	—	0.977	−0.977	0.785	1.128	−1	0.999
L_{17}	1.414	—	—	—	0.032	−0.032	0	—	—	—
L_{18}	1.414	—	—	—	1.382	1.382	—	1.414	1.414	—
L_{19}	1	—	—	—	0.023	0.023	—	—	—	—
L_{20}	1	—	—	—	0.023	0.023	—	—	—	—

Table 2
Comparison of NPF and NLF approaches.

NO.	V	t /s	ξ_V /%	ξ_t /%
OSW	62	2.6	—	—
OSN-NPF	64.277	2.7	—	—
OSN-NLF	65.571	3.0	2.013	11.111
OSNL-NPF	68.880	14.5	—	—
OSNL-NLF	71.252	25.8	3.444	77.931

Note: $\xi_V = \dfrac{V_{NLF} - V_{NNF}}{V_{NNF}} \times 100\%$; $\xi_t = \dfrac{t_{NLF} - t_{NNF}}{t_{NNF}} \times 100\%$

3.2. 3D L-shape structure

A typical 3D L-shape design domain provides a further indication of the range of applicability of the proposed approaches, as shown in Fig. 7a, where L is taken as unity (this problem has also been considered by Tyas [41] and Kocvara [24]). Pinned supports are present on the top face and two unity point loads are applied downwards at the tip of 'L'. Both limiting tensile and compressive stresses are taken as unity. The design domain is discretized using 28 neighboring nodes (Fig. 7b) connected by 138 potential bars to generate a ground structure (Fig. 7c). The optimized structures are shown in Fig. 7 d-h. In Fig. 7, OSW, OSN-NPF, OSN-NLF, OSNL-NPF, and OSNL-NLF represent optimized structure without stability, optimized structure with nodal stability using NPF approach, optimized structure with nodal stability using NLF approach, optimized structure with nodal and local buckling stability using NPF approach, optimized structure with nodal and bar local buckling stability using NLF approach. The computation times and the volumes of the optimized structures using the NPF and NPF approaches are shown in Table 2.

When nodal stability considerations are neglected and a linear programming solver is employed, the optimized structure is shown in Fig. 7d, with a volume of 62 and an optimization time of 2.6 s. When only the nodal stability is considered using the NPF approach, the optimized structure is shown in Fig. 7e with a volume of 64.277 m^3 and an optimization time of 2.7 s. When only the nodal stability is considered using the NLF approach, the optimized structure is shown in Fig. 7f. As can be seen from Fig. 7e and Fig. 7f, both structures do not have nodal stability problems. However, the volume of the optimized structure by using the NLF approach is 11.111% more than the volume of the optimized structure by using the NPF approach. This is mainly because, in the NLF method, only compression bars are considered when calculating the nominal forces. As a result, the stable nodes may be judged as unstable nodes thus adding unnecessary bracings. In contrast, in the NPF approach, the influence of both the tension bar and the compression bar connecting the nodes is considered when calculating the nominal force, making the calculation more accurate. When nodal stability and local buckling stability of the bar are considered simultaneously, the results of optimization using the NLF approach and using the NPF approach are shown in Fig. 7f and g, respectively. As shown in Table 2, the computation time using the NLF approach is 77.931% more than the NPF approach, which is mainly due to the small number of optimization variables in the nominal perturbing force method. It is worth noting that in the optimized structures, some unbraced nodes may be contained within the consecutive tension bars, which may make the structure unstable. However, unlike the unbraced nodes within consecutive compression bars, these unbraced nodes can be eliminated directly and then merge with consecutive tension bars into a single long bar in the in-depth design stage.

The magnitudes of the axial forces of all the compression bars in the optimized structures OSNL-NPF and OSNL-NLF are compared with their critical buckling forces, as shown in Fig. 8. In optimized structures, the magnitude of the axial force of the compression bar is not greater than its critical buckling force, regardless of whether the nominal lateral force method or the nominal perturbing force method is used. This shows the effectiveness of the method proposed in this paper to address the local buckling problem.

This numerical example shows that the NPF approach proposed in this paper has a better optimization effect and higher optimization efficiency compared with the traditional NLF approach. In addition, the ASI approach proposed in this paper to address the local buckling problem in topology optimization is effective.

3.3. 3D crane structure

A 3D crane design domain example is studied in this section, as shown in Fig. 9a, where L is 0.2 m (this problem has also been considered by Smith [39] and Zegard [46]). As shown in Fig. 9a, in the design domain, pinned supports are present on the bottom face and four-point loads $P = 20$ kN is applied downwards at the tip of the upper beam. Limiting tensile and compressive stresses are taken as 355 MPa. The design domain is discretized using 38 neighboring nodes (Fig. 9b) connected by 173 potential bars to generate an adjacent connectivity ground structure (Fig. 9c).

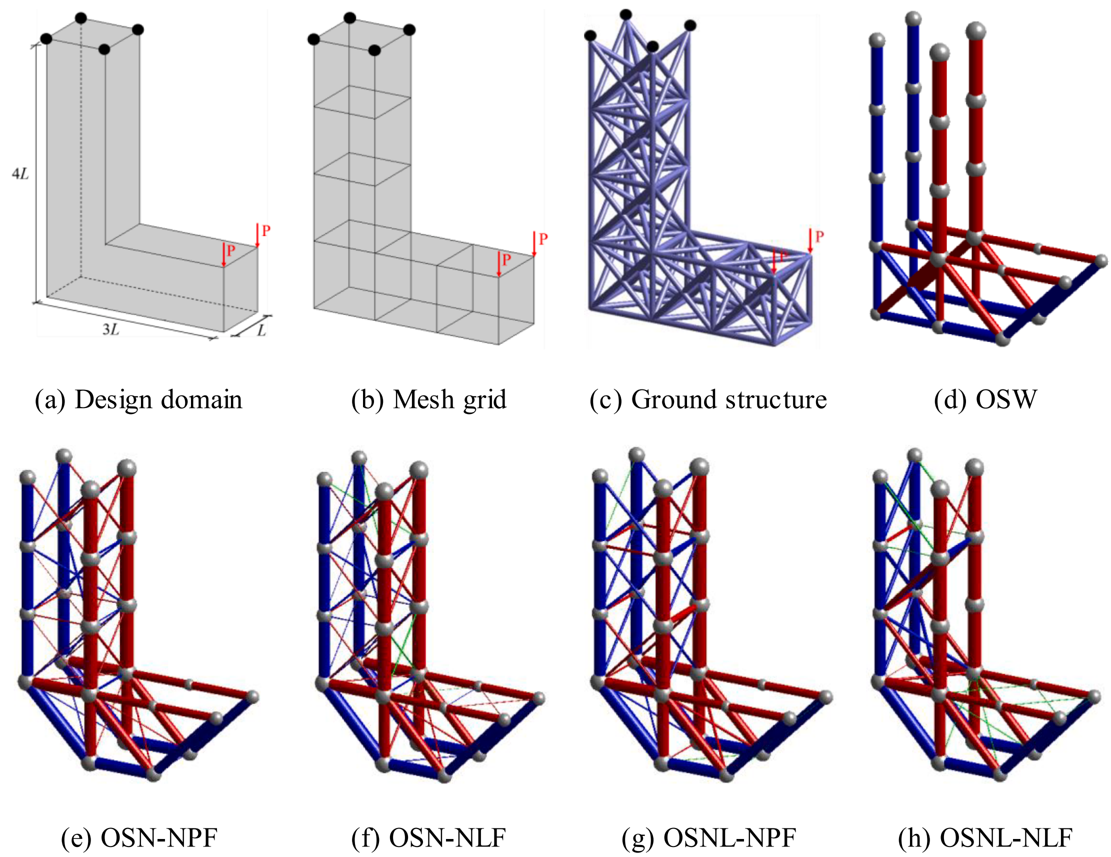

Fig. 7. Optimization of L-shaped structure. Note: OSW, OSN-NPF, OSN-NLF, OSNL-NPF, and OSNL-NLF represent optimized structure without stability, optimized structure with nodal stability using NPF approach, optimized structure with nodal stability using NLF approach, optimized structure with nodal and local buckling stability using NPF approach, optimized structure with nodal and bar local buckling stability using NLF approach.

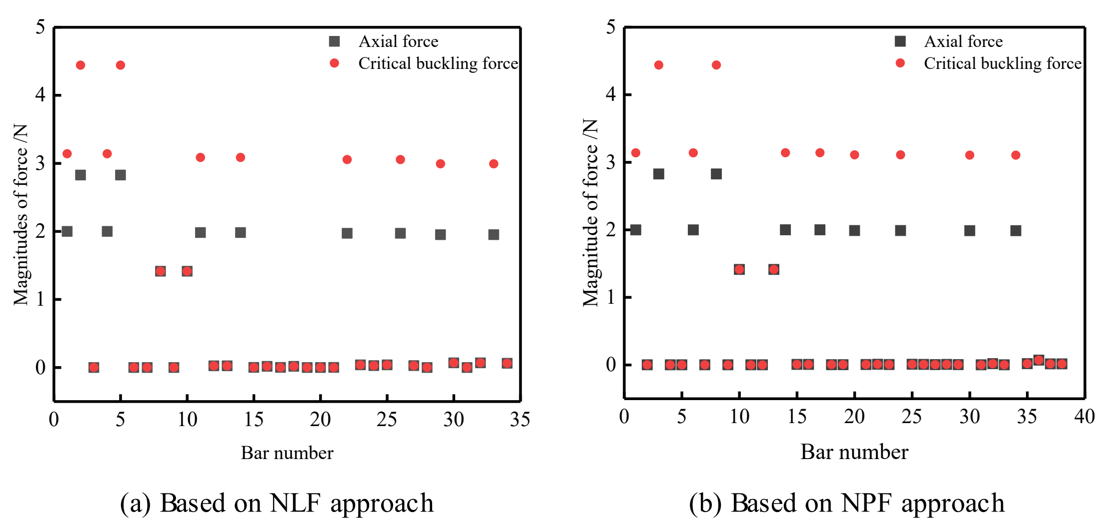

Fig. 8. Comparison of axial force and critical buckling force of L-shaped structure.

The optimized structure with a volume of $V_{OSW} = 2.428 \times 10^6$ mm^3 is shown in Fig. 9d when neither the nodal stability nor local buckling stability is considered in the optimization. However, almost all the nodes within compressive bars are unstable, which cannot be used in practical applications, obviously. As shown in Fig. 9e, when only the nodal local buckling stability is considered in the optimization, an optimized structure with a volume of $V_{OSN} = 2.635 \times 10^6$ mm^3 is obtained, where $\frac{V_{OSN}-V_{OSW}}{V_{OSW}} \times 100\backslash\% = 8.526\backslash\% = 8.526\{\%$ more material is used to make the nodes stable. As shown in Fig. 9f, an optimized structure with volume $V_{OSNL} = 5.607 \times 10^6$ mm^3 is obtained with both nodal and local buckling stability, where $\frac{V_{OSNB}-V_{OSW}}{V_{OSW}} \times 100\backslash\% = 130.931\backslash\% = 130.931\{\%$ more material is used to make the nodes and local buckling stable.

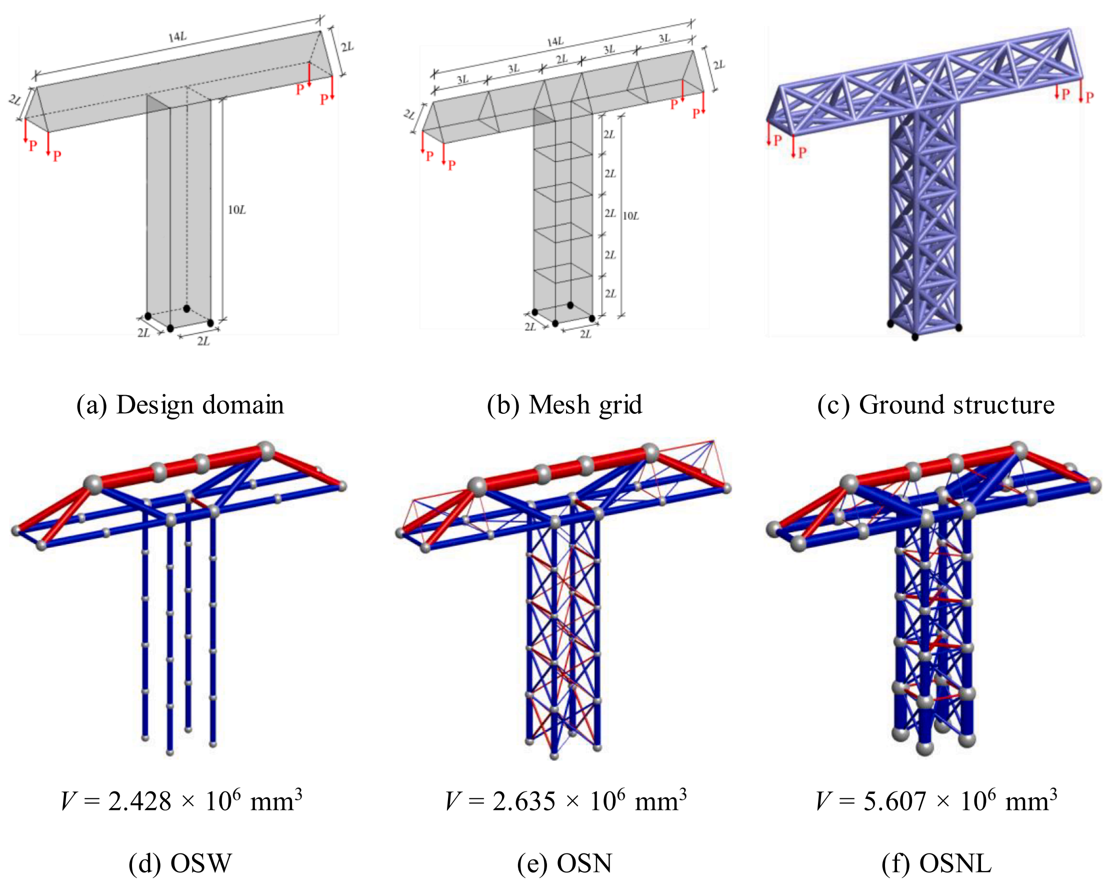

Fig. 9. Optimization of crane. Note: OSW, OSN, and OSNL represent optimized structure without stability, optimized structure with nodal stability, and optimized structure with nodal stability and local buckling stability, respectively.

Fig. 10 shows two comparisons of the axial and critical buckling forces of the optimized structures. As shown in Fig. 10a, when local buckling stability is not considered, the magnitudes of the axial forces of many bars in the optimized structure exceed their critical buckling forces. When local buckling is considered in the optimization using the ASI method, the axial force and critical local buckling force of all compression bars in the optimized structure are shown in Fig. 10 b. It can be seen from Fig. 10b that the magnitudes of the axial forces of all the compression bars do not exceed their critical buckling forces, which demonstrates the effectiveness of the ASI method proposed in this study.

4. Conclusions

The main contribution of this study is the development of a truss topology optimization formulation including nodal and local buckling stability constraints. A brief review of literature has shown that a

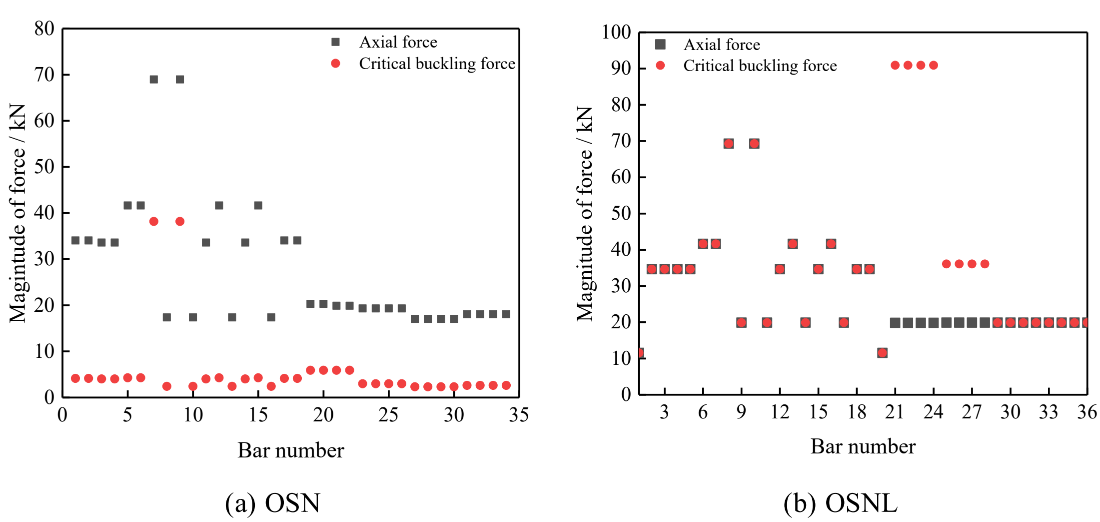

Fig. 10. Comparison of axial force and critical buckling force of the crane.

convenient approach to state the basic plastic problem of truss topology optimization relies on the FELA method.

The novel nominal perturbing force (NPF) approach has been proposed to address the nodal instability in the truss topology optimization problem. In the NPF approach, nominal perturbing forces consistent with the directions of the Cartesian axes are used to model the possible perturbations of the unstable nodes. Compared with the conventional nominal lateral force (NLF) approach, (a) the NPF approach has higher computational efficiency because it contains fewer optimization variables; (b) the effect of tension bars connected to the nodes is considered in determining the unstable nodes, which can lead to a better optimization result.

In addition, the novel nominal allowable stress iteration (ASI) approach is proposed to address the local buckling instability in the truss topology optimization problem. In this way, the concave local buckling instability problem is linearized in each iteration and can be solved efficiently by a linear programming solver. Numerical examples have shown the practical applicability of the proposed method for the preliminary design of truss structures.

The proposed method is readily applicable and allows some extensions. Since Euler's criterion for the local buckling stability overestimates the critical buckling strength of the bar, other criteria based on design codes should be considered for more accuracy.

Funding

This research is financially supported by the National Natural Science Foundation of China (Grant numbers: 51978151, 51778283), the Scholarship of China National Scholarship Council (201806090265), the Scientific Research Foundation of Graduate School of Southeast University (Grant number: YBPY1958).

Declaration of Competing Interest

The authors declare that they have no known competing financial interests or personal relationships that could have appeared to influence the work reported in this paper.

References

[1] Achtziger W. Local stability of trusses in the context of topology optimization - Part I: Exact modelling. Struct Optim 1999;17(4):235–46.
[2] Ben-Tal A, Nemirovski A. Robust truss topology design via semidefinite programming. SIAM J Optim 1997;7(4):991–1016.
[3] Ben A, Laurent T, Ghaoui E, and Nemirovski A. Robust Semidefinite Programming. handbook on semidefinite programming kluwer academis publishers 1998.
[4] Bendse MP, Sigmund O. Topology Optimization: Theory, Method and Applications. Springer; 2003.
[5] Cai Q, He L, Xie Y, Feng R, Ma J. Simple and effective strategies to generate diverse designs for truss structures. Structures 2021;32:268–78.
[6] Cerveira A, Agra A, Bastos F, Gromicho J. A new Branch and Bound method for a discrete truss topology design problem. Comput Optim Appl 2013;54(1):163–87.
[7] China MoHaU-RDotPsRo, National Standard (Mandatory) of the People's Republic of China, Standard for design of steel structures. China Architecture & Building Press, 2017.
[8] China MoHaU-RDotPsRo, National Standard (Mandatory) of the People's Republic of China, Standard for design of steel structures. China Architecture & Building Press, 2017.
[9] Damkilde L, Hoyer O. An efficient implementation of limit state calculations based on lower-bound solutions. Comput Struct 1993;49(6):953–62.
[10] Descamps B, Coelho RF. The nominal force method for truss geometry and topology optimization incorporating stability considerations. Int J Solids Struct 2014;51(13):2390–9.
[11] Dorn W, Gomory R, Greenberg H. Automatic design of optimal structures. Journal de Mécanique 1964;3 25-52.
[12] Duan Z, Yan J, Lee I, Lund E, Wang J. Discrete material selection and structural topology optimization of composite frames for maximum fundamental frequency with manufacturing constraints. Struct Multidiscip Optim 2019;60(5):1741–58.
[13] Guo X, Cheng GD, Olhoff N. Optimum design of truss topology under buckling constraints. Struct Multidiscip Optim 2005;30(3):169–80.
[14] He L, Gilbert M. Rationalization of trusses generated via layout optimization. Struct Multidiscip Optim 2015;52(4):677–94.
[15] He LW, Gilbert M, Johnson T, Pritchard T. Conceptual design of AM components using layout and geometry optimization. Comput Math Appl 2019;78(7):2308–24.
[16] He Y, Cai K, Zhao Z-L, Xie YM. Stochastic approaches to generating diverse and competitive structural designs in topology optimization. Finite Elem Anal Des 2020;173:103399.
[17] Institute BS, Eurocode 3: Part 1. Design of steel structures, general rules and rules for buildings, 1992.
[18] Institute BS, BS 5950: Part 1. Structural use of steelwork in building. Code of practice for design., Rolled and welded sections. British Standards Institute, 2000.
[19] Kaveh, and A., Advances in Metaheuristic Algorithms for Optimal Design of Structures (3rd edition), Switzerland: Springer International Publishing; 2021.
[20] Kaveh A, Kalatjari V. Topology optimization of trusses using genetic algorithm, force method and graph theory. Int J Numer Meth Eng 2003;58(5):771–91.
[21] Kaveh A, Zolghadr A. Topology optimization of trusses considering static and dynamic constraints using the CSS. Appl Soft Comput 2013;13(5):2727–34.
[22] Kaveh A, Ahmadi B. Sizing, geometry and topology optimization of trusses using force method and supervised charged system search. Struct Eng Mech 2014;50(3):365–82.
[23] Kaveh A, Hassani B, Shojaee S, Tavakkoli SM. Structural topology optimization using ant colony methodology. Eng Struct 2008;30(9):2559–65.
[24] Kocvara M. On the modelling and solving of the truss design problem with global stability constraints. Struct Multidiscip Optim 2002;23(3):189–203.
[25] Krabbenhoft K, Damkilde L, Krabbenhoft S. Ultimate limit state design of sheet pile walls by finite elements and nonlinear programming. Comput Struct 2005;83(4–5):383–93.
[26] Krabbenhoft K, Lyamin AV, Sloan SW. Three-dimensional Mohr-Coulomb limit analysis using semidefinite programming. Commun Numer Methods Eng 2008;24(11):1107–19.
[27] Lemonge ACC, Carvalho JPG, Hallak PH, Vargas DEC. Multi-objective truss structural optimization considering natural frequencies of vibration and global stability. Expert Syst Appl 2021;165:113777.
[28] Liu F, Feng R, Tsavdaridis KD, Yan G. Designing efficient grid structures considering structural imperfection sensitivity. Eng Struct 2020;204:109910.
[29] Ma JM, Li Z, Zhao ZL, Xie YM. Creating novel furniture through topology optimization and advanced manufacturing. Rapid Prototyp J 2021;27(9):1749–58.
[30] Ma J, Zhao Z-L, Lin S, Xie YM. Topology of leaf veins: Experimental observation and computational morphogenesis. J Mech Behav Biomed Mater 2021;123:104788.
[31] Mela K. Resolving issues with member buckling in truss topology optimization using a mixed variable approach. Struct Multidiscip Optim 2014;50(6):1037–49.
[32] Nishino T, Kato J. Robust topology optimization based on finite strain considering uncertain loading conditions. Int J Numer Meth Eng 2021;122(6):1427–55.
[33] Ohsaki M, Optimization of finite dimensional structures: Optimization of finite dimensional structures; 2011.
[34] Ohsaki M, Katoh N. Topology optimization of trusses with stress and local constraints on nodal stability and member intersection. Struct Multidiscip Optim 2005;29(3):190–7.
[35] Poulsen PN, Damkilde L. Limit state analysis of reinforced concrete plates subjected to in-plane forces. Int J Solids Struct 2000;37(42):6011–29.
[36] Poulsen PN, Olesen JF, Baandrup M. Truss optimization applying finite element limit analysis including global and local stability. Struct Multidiscip Optim 2020;62(1):41–54.
[37] Rahami H, Kaveh A, Gholipour Y. Sizing, geometry and topology optimization of trusses via force method and genetic algorithm. Eng Struct 2008;30(9):2360–9.
[38] Rozvany GIN. Difficulties in truss topology optimization with stress, local buckling and system stability constraints. Structural Optimization 1996;11(3–4):213–7.
[39] da Silva Smith O. Generation of ground structures for 2D and 3D design domains. Eng Comput 1998;15(4):462–500.
[40] Somekh E, Kirsch U. Interactive optimal-design of truss structures. Comput Aided Des 1981;13(5):253–9.
[41] Tyas A, Gilbert M, Pritchard T. Practical plastic layout optimization of trusses incorporating stability considerations. Comput Struct 2006;84(3–4):115–26.
[42] Wang B, Zhou Y, Zhou YM, Xu SL, Niu B. Diverse competitive design for topology optimization. Struct Multidiscip Optim 2018;57(2):891–902.
[43] Winter G. Lateral Bracing of Columns and Beams. T Am Soc Civ Eng 1960;125(1):807–26.
[44] Yura JA. Winter's bracing approach revisited. Eng Struct 1996;18(10):821–5.
[45] Zegard T, Paulino GH. GRAND - Ground structure based topology optimization for arbitrary 2D domains using MATLAB. Struct Multidiscip Optim 2014;50(5):861–82.
[46] Zegard T, Paulino GH. GRAND3-Ground structure based topology optimization for arbitrary 3D domains using MATLAB. Struct Multidiscip Optim 2015;52(6):1161–84.
[47] Zhao Z, Yu D, Zhang T, Zhang Ni, Liu H, Liang B, et al. Efficient form-finding algorithm for freeform grid structures based on inverse hanging method. J Build Eng 2022;46:103746.
[48] Zhao Z, Wu J, Qin Y, Liang B. The strong coupled form-finding and optimization algorithm for optimization of reticulated structures. Adv Eng Softw 2020;140:102765.
[49] Zhao ZW, Chen ZH, Yan XY, Xu H, Zhao BZ. Simplified numerical method for latticed shells that considers member geometric imperfection and semi-rigid joints. Adv Struct Eng 2016;19(4):689–702.